

Correlated many-body calculation to study characteristics of Shannon information entropy for ultracold trapped interacting bosons

Sudip Kumar Haldar,¹ Barnali Chakrabarti,² Tapan Kumar Das,³ and Anindya Biswas⁴

¹*Department of Physics, Lady Brabourne College, P 1/2 Suhrawardy Avenue, Kolkata 700017, India*

²*Department of Physics, Kalyani University, Kalyani, Nadia, West Bengal, India, Pin: 741235*

³*Department of Physics, University of Calcutta, 92 A.P.C. Road, Kolkata-700009, India*

⁴*Harish-Chandra Research Institute, Chhatnag Road, Jhansi, Allahabad-211019, India*

(Received 18 April 2013; revised manuscript received 25 July 2013; published 3 September 2013)

A correlated many-body calculation is presented to characterize the Shannon information entropy of trapped interacting bosons. We reformulate the one-body Shannon information entropy in terms of the one-body probability density. The minimum limit of the entropy uncertainty relation is approached by making N very small in our numerical work. We examine the effect of correlations in the calculation of information entropy. Comparison with the mean-field result shows that the correlated basis function is indeed required to characterize the important features of the information entropies. We also accurately calculate the point of critical instability of an attractive BEC, which is in close agreement with the experimental value. Next, we calculate two-body entropies in position and momentum spaces and study quantum correlations in the attractive BEC.

DOI: [10.1103/PhysRevA.88.033602](https://doi.org/10.1103/PhysRevA.88.033602)

PACS number(s): 03.75.Hh, 89.70.Cf

I. INTRODUCTION

In recent years, the information theoretic methods play an interesting and important role in the study of quantum mechanical systems such as nuclei, atomic cluster, confined atoms, etc. [1–6]. The extraction of probability densities in both the position and momentum spaces and the associated calculation of information entropy provide some additional relevant information of the system. Recent experimental achievement of Bose-Einstein condensation (BEC) in the dilute alkali atomic vapor [7–9] opens a new avenue of research in this direction. The system of ultracold trapped atoms obey Bose-Einstein statistics and a finite fraction of particles condense to the ground state below the critical temperature. The accumulated atoms in the single state can be described as a single quantum particle having nonlinear interaction. The presence of an external harmonic trapping potential allows for measurement both in the coordinate and momentum spaces. The interparticle interaction and the confining potential strongly influence the static and dynamic properties of the condensate. Correlations among the atoms in the external trap also play a key role even though the laboratory BEC is extremely dilute.

In this paper, we present the results of numerical studies of Shannon information entropy of ultracold trapped interacting bosons in both the coordinate and momentum spaces. We adopt a two-body correlated basis function together with the realistic van der Waals potential for the description of the condensate at zero temperature. From the condensate wave function we calculate the one-body density $R_1(\vec{r}_k)$ and two-body density function $R_2(r_{ij})$, where \vec{r}_k is the distance of the k th boson from the center of mass of the condensate and r_{ij} is the relative separation of the (ij) pair of bosons. The Shannon entropy in position space is defined as

$$S_r = - \int \rho(\vec{r}) \ln \rho(\vec{r}) d\vec{r}, \quad (1)$$

where $\rho(\vec{r})$ is either the one body or the pair density in the coordinate space. The momentum space Shannon entropy is described in similar way as

$$S_p = - \int \phi(\vec{p}) \ln \phi(\vec{p}) d\vec{p}, \quad (2)$$

where $\phi(\vec{p})$ represents the one-body or pair-momentum density. $\rho(\vec{r})$ and $\phi(\vec{p})$ are normalized to unity. Throughout this paper, we adopt the units, referred to as the oscillator units (o.u.), in which length and energy are expressed in units of $a_{ho} = \sqrt{\frac{\hbar}{m\omega}}$ and $\hbar\omega$, respectively, ω being trapping frequency. As densities are measured in this unit, all the entropy values presented here are also in o.u. The Shannon information entropies basically measure the uncertainty of the probability distribution in the respective spaces. Using the position and momentum space entropies (S_r and S_p , respectively), Bialynicki-Birula and Mycielski (BBM) derived a stronger version of the Heisenberg uncertainty relation [10]. For a three-dimensional system, the total entropic sum has the form

$$S = S_r + S_p \geq 3[1 + \ln(\pi)] \simeq 6.434. \quad (3)$$

This means that the conjugate position and momentum space information entropies S_r and S_p maintain an inverse relationship with each other. It signifies that when a system is strongly localized in position space, the corresponding information entropy and uncertainty in position space decreases. The corresponding momentum distribution becomes delocalized, therefore the information entropy and uncertainty in momentum space increases. It is important to note that the BBM inequality [Eq. (3)] presents a lower bound and the equality is maintained for a Gaussian wave function.

It is to be noted that information theory of correlated bosons in the external trap has been studied using uncorrelated mean-field theory [11]. The universal expression for the total entropy in different quantum systems takes the form

$S = a + b \ln N$, where a and b are the parameters that depend on the given system [2]. Although the choice of our system is quite similar to that of earlier studies, but the motivation of our present work is quite different and is as follows. First: As the interacting bosons in the external trap are correlated, the uncorrelated mean-field Gross-Pitaevskii (GP) equation may not reveal the correct information and characteristic features in the measures of Shannon entropy. In the GP equation, the interparticle interaction is taken as a contact interaction, whose strength is given by a single parameter a_s , the s -wave scattering length. However, the importance of a realistic, finite-range interaction has been pointed out [12,13]. Hence, the presence of a long attractive tail in a realistic interaction, such as the van der Waal interaction will have important contributions to correlation function and will provide more realistic aspects. Thus, our present calculation, keeping all possible two-body correlations and realistic interatomic interaction will provide more accurate results than those obtained from GP and we may observe new features in the calculation of Shannon entropy and correlation properties of the confined bosons. Second: For the repulsive condensate, a_s is positive, therefore with increase in a_s or increase in number of bosons N , the effective interaction parameter Na_s increases. Thus, for the repulsive condensate, with increase in Na_s the system becomes less correlated, as the central density decreases. However, for attractive condensate $a_s < 0$, the trend is in the opposite direction. It is well known that for attractive BEC, the condensate collapses when N becomes equal to some critical number N_{cr} . Thus, when N is close to but less than N_{cr} , the condensate is highly correlated and for $N \geq N_{cr}$ the condensate collapses. This is a very crucial point where the study of information entropy may provide some new characteristic features of Shannon entropy, and from that we may get very accurate value of the stability factor which is experimentally known [8]. This is beyond the scope of study of the mean-field GP equation. We will also introduce correlation features to study the correlation properties of the attractive condensate.

This paper is organized as follows. In Sec. II, we briefly review our theoretical approach. In Sec. III, we present our calculation and results of information entropy of the one-body density, entropy uncertainty relation (EUR), and the universal property of total entropy. This section also presents results of pair correlation and Shannon information entropy of two-body density and statistical correlation function. Finally, in Sec. IV, we draw our conclusions.

II. METHODOLOGY

A. Many-body calculation with correlated potential harmonic basis

In this work, we have employed our newly developed correlated potential harmonic expansion method (CPHEM) which we have successfully used in our earlier studies of different properties of condensate [14–18]. Here, we briefly describe the method. Details can be found in Refs. [19–21].

We consider a system of N identical bosons interacting through a two-body potential $V(\vec{r}_{ij}) = V(\vec{r}_i - \vec{r}_j)$ and confined in an external harmonic potential of frequency ω . The time-independent quantum many-body Schrödinger equation

is given by

$$\left[-\frac{\hbar^2}{2m} \sum_{i=1}^N \nabla_i^2 + \sum_{i=1}^N V_{\text{trap}}(\vec{r}_i) + \sum_{i,j>i}^N V(\vec{r}_i - \vec{r}_j) - E \right] \times \Psi(\vec{r}_1, \dots, \vec{r}_N) = 0, \quad (4)$$

where m is the mass of each boson, E the energy of the condensate, and the trapping potential $V_{\text{trap}}(\vec{r}_i) = \frac{1}{2}m\omega^2 r_i^2$. We can eliminate the center-of-mass motion by using the standard Jacobi coordinates [22–24] defined as

$$\vec{\zeta}_i = \sqrt{\frac{2i}{i+1}} \left(\vec{r}_{i+1} - \frac{1}{i} \sum_{j=1}^i \vec{r}_j \right) \quad (i = 1, \dots, \mathcal{N}). \quad (5)$$

The center-of-mass coordinate is $\vec{R} = \frac{1}{N} \sum_{i=1}^N \vec{r}_i$. The relative motion of the bosons is given by

$$\left[-\frac{\hbar^2}{m} \sum_{i=1}^{\mathcal{N}} \nabla_{\zeta_i}^2 + V_{\text{trap}} + V_{\text{int}}(\vec{\zeta}_1, \dots, \vec{\zeta}_{\mathcal{N}}) - E_R \right] \times \Psi(\vec{\zeta}_1, \dots, \vec{\zeta}_{\mathcal{N}}) = 0, \quad (6)$$

where $\mathcal{N} = N - 1$. Here, V_{trap} is the effective trapping potential and $V_{\text{int}}(\vec{\zeta}_1, \dots, \vec{\zeta}_{\mathcal{N}})$ is the sum of all pairwise interactions expressed in terms of Jacobi coordinates. $E_R (= E - \frac{3}{2}\hbar\omega)$ is the relative energy of the system.

Hyperspherical harmonic expansion method (HHEM) is an *ab initio* many-body tool to solve the many-body Schrödinger equation. The hyperspherical variables are constituted by the hyperradius $r = \sqrt{\sum_{i=1}^{\mathcal{N}} \zeta_i^2}$ and $(3\mathcal{N} - 1)$ hyperangular variables which are comprised of $2\mathcal{N}$ spherical polar angles $(\vartheta_j, \varphi_j; j = 1, \dots, \mathcal{N})$ associated with \mathcal{N} Jacobi vectors and $(\mathcal{N} - 1)$ hyperangles $(\phi_2, \phi_3, \dots, \phi_{\mathcal{N}})$ giving their relative lengths. The total wave function is expanded in the complete set of hyperspherical harmonic (HH) functions [23]. Therefore, HHEM is a complete many-body approach and includes all possible correlations. However, there are serious difficulties for a large number of particles. The calculation of potential matrix elements of all pairwise potentials becomes a formidable task and the convergence rate of the hyperspherical harmonic expansion becomes extremely slow in the large particle limit, due to rapidly increasing degeneracy of the basis. For these reasons, HHEM can be used for the three-body systems only and it is not suitable for the description of the experimental BEC containing a few thousand to a few million particles. However, for the achievement of a stable BEC in the laboratory, the atomic cloud must be extremely dilute physically, so as to preclude three-body collisions, which lead to molecule formation and consequent depletion [25]. Hence, the interparticle separation must be very large compared to the range of the effective potential (which is $|a_s|$). Thus, $n|a_s|^3 \ll 1$, where n is the number density $\sim N/(a_{ho})^3$, with a_{ho} being the oscillator length of the trap. In the original JILA experiment, $a_s/a_{ho} = 0.00433$ and this condition is well satisfied by N up to $\sim 10^6$. As a consequence, three- and higher-body correlations are not relevant in the condensate wave function Ψ . Now, as only two-body interactions are present, Ψ can be decomposed into Faddeev components. Since only two-body correlations are relevant, the Faddeev component corresponding to the (ij) -interacting pair is a function of

\vec{r}_{ij} and r only and can be expanded in the subset of HH, called the potential harmonics (PH) subset, which is sufficient for the expansion of $V(\vec{r}_{ij})$, as a function of hyperspherical variables [19,20]. This leads to a dramatic simplification: For any N , the active degrees of freedom is effectively reduced to only four, viz., \vec{r}_{ij} and r for each of the $N(N-1)/2$ Faddeev components (the remaining irrelevant degrees of freedom in the dilute condensate being frozen). Since Ψ is decomposed into all interacting pair Faddeev components, all two-body correlations are included. The emerging picture for a given Faddeev component is that when two particles interact, the rest of the particles in the condensate behave simply as inert spectators. The fact that *only a few degrees of freedom are relevant* is consistent with the collective motion of the condensate as a single quantum entity.

Thus, we decompose the total wave function Ψ into two-body Faddeev components for all interacting pairs as

$$\Psi = \sum_{i,j>i}^N \phi_{ij}(\vec{r}_{ij}, r). \quad (7)$$

As we discussed earlier, due to the presence of two-body correlations only, ϕ_{ij} is a function of interacting-pair separation (\vec{r}_{ij}) and the global hyperradius r only. ϕ_{ij} is symmetric under P_{ij} for bosons and satisfies the Faddeev equation

$$[T + V_{\text{trap}} - E_R]\phi_{ij} = -V(\vec{r}_{ij}) \sum_{k,l>k}^N \phi_{kl}, \quad (8)$$

where $T = -\frac{\hbar^2}{m} \sum_{i=1}^N \nabla_{\zeta_i}^2$ is the total kinetic energy. Applying the operator $\sum_{i,j>i}$ on both sides of Eq. (8), we get back the original Schrödinger equation. In this approach, we assume that when the (ij) pair interacts, the rest of the bosons are inert spectators. Thus, the total hyperangular momentum quantum number as also the orbital angular momentum of the whole system is contributed by the interacting pair only. Next, we expand ϕ_{ij} in the PH subset

$$\phi_{ij}(\vec{r}_{ij}, r) = r^{-\frac{3(N-1)}{2}} \sum_K \mathcal{P}_{2K+l}^{lm}(\Omega_{\mathcal{N}}^{ij}) u_K^l(r). \quad (9)$$

$\Omega_{\mathcal{N}}^{ij}$ denotes the full set of hyperangles in the $3\mathcal{N}$ -dimensional space for the (ij) partition, in which the (ij) pair interacts and $\mathcal{P}_{2K+l}^{lm}(\Omega_{\mathcal{N}}^{ij})$ is a member of the PH basis. It has an analytic expression [22] given by

$$\mathcal{P}_{2K+l}^{l,m}(\Omega_{\mathcal{N}}^{(ij)}) = Y_{lm}(\omega_{ij})^{(\mathcal{N})} P_{2K+l}^{l,0}(\phi) \mathcal{Y}_0(D-3), \quad (10)$$

$$D = 3\mathcal{N}$$

$\mathcal{Y}_0(D-3)$ is the HH of order zero in the $(3\mathcal{N}-3)$ dimensional space spanned by $\{\zeta_1, \dots, \zeta_{\mathcal{N}-1}\}$ Jacobi vectors; ϕ is the hyperangle given by $r_{ij} = r \cos \phi$. For the remaining $(\mathcal{N}-1)$ noninteracting bosons, we define a hyperradius as

$$\rho_{ij} = \sqrt{\sum_{k=1}^{\mathcal{N}-1} \zeta_k^2} = r \sin \phi \quad (11)$$

so that $r^2 = r_{ij}^2 + \rho_{ij}^2$. The relevant set of $(3\mathcal{N}-1)$ quantum numbers of HH is now reduced to *only* three and the remaining

ones vanish:

$$l_1 = l_2 = \dots = l_{\mathcal{N}-1} = 0, \quad (12)$$

$$m_1 = m_2 = \dots = m_{\mathcal{N}-1} = 0, \quad (13)$$

$$n_2 = n_3 = \dots = n_{\mathcal{N}-1} = 0, \quad (14)$$

and for the interacting pair $l_{\mathcal{N}} = l$, $m_{\mathcal{N}} = m$, and $n_{\mathcal{N}} = K$. Thus, the $3\mathcal{N}$ -dimensional Schrödinger equation reduces effectively to a four-dimensional equation with the relevant set of quantum numbers: principal quantum number n , orbital angular momentum quantum number l , azimuthal quantum number m , and grand orbital quantum number $2K+l$ for any N . Substituting Eq. (9) into (8) and projecting on a particular PH, a set of coupled differential equations (CDE) for the partial wave $u_K^l(r)$ is obtained as

$$\left[-\frac{\hbar^2}{m} \frac{d^2}{dr^2} + V_{\text{trap}}(r) + \frac{\hbar^2}{mr^2} \{ \mathcal{L}(\mathcal{L}+1) + 4K(K+\alpha+\beta+1) \} - E_R \right] U_{Kl}(r) + \sum_{K'} f_{Kl} V_{KK'}(r) f_{K'l} U_{K'l}(r) = 0, \quad (15)$$

where $\mathcal{L} = l + \frac{3N-6}{2}$, $U_{Kl} = f_{Kl} u_K^l(r)$, $\alpha = \frac{3N-8}{2}$, and $\beta = l + 1/2$. f_{Kl} is a constant and represents the overlap of the PH for interacting partition with the sum of PHs corresponding to all partitions [24]. The potential matrix element $V_{KK'}(r)$ is given by

$$V_{KK'}(r) = \int \mathcal{P}_{2K+l}^{lm*}(\Omega_{\mathcal{N}}^{ij}) V(r_{ij}) \mathcal{P}_{2K'+1}^{l'm}(\Omega_{\mathcal{N}}^{ij}) d\Omega_{\mathcal{N}}^{ij}. \quad (16)$$

B. Introduction of a short-range correlation function

As the two-body interaction is represented by a contact interaction, whose strength is given by the s -wave scattering length a_s only, the mean-field GP equation completely disregards the detailed structure of the interatomic potential. The sign of a_s determines nature of the interaction: a positive (negative) value of a_s represents the repulsive (attractive) interaction. But, in realistic interatomic interactions, such as the van der Waals potential, there is always an attractive $-\frac{C_6}{r_{ij}^6}$ type tail part at large separations and a strong repulsion at short separations [26]. Depending on the nature of these two parts, a_s can either be positive or negative. In an earlier many-body calculation [27], we observed an appreciable effect of shape dependence of the interatomic interaction, for larger values of N , even for the dilute condensate. Moreover, in the mean-field GP equation for an attractive condensate, the Hamiltonian is unbound from below and an approximate solution is obtained only in the metastable region. So, in our present many-body calculation, we use a realistic interatomic potential, viz., the van der Waals (vdW) potential with a hard core [26].

The strong short-range repulsion of the realistic potential produces a short-range correlation in the (ij) interacting pair Faddeev component ϕ_{ij} , which forbids the interacting pair to come too close. To include the effect of this strong repulsion, we introduce an additional short-range correlation function (SRCF) $\eta(r_{ij})$ in the PH expansion basis for ϕ_{ij} . The SRCF is obtained as the zero-energy solution of the interacting pair

Schrödinger equation

$$-\frac{\hbar^2}{m} \frac{1}{r_{ij}^2} \frac{d}{dr_{ij}} \left(r_{ij}^2 \frac{d\eta(r_{ij})}{dr_{ij}} \right) + V(r_{ij})\eta(r_{ij}) = 0. \quad (17)$$

The asymptotic form of $\eta(r_{ij})$ quickly attains $C(1 - a_s/r_{ij})$, from which a_s is calculated [26]. The hard-core radius of the vdW potential is adjusted to give the appropriate value of a_s . This ensures that the short-range repulsion is correctly accounted for. The inclusion of SRCF has the same effect as the Jastrow function in other many-body approaches. The zero-energy two-body wave function $\eta(r_{ij})$ is a good representation of the short-range behavior of ϕ_{ij} , as in the experimental BEC the energy of the interacting pair is negligible compared with the depth of the interatomic potential. Since $\eta(r_{ij})$ has the correct short-separation behavior of the (ij) interacting pair, the $r_{ij} \rightarrow 0$ behavior of ϕ_{ij} is correctly reproduced [21]. As a result, the rate of convergence of the PH expansion is dramatically enhanced.

With the inclusion of SRCF, we replace Eq. (9) by

$$\phi_{ij}(\vec{r}_{ij}, r) = r^{-\frac{3N-1}{2}} \sum_K \mathcal{P}_{2K+1}^{lm}(\Omega_N^{ij}) u_K^l(r) \eta(r_{ij}), \quad (18)$$

and the correlated PH (CPH) basis function is given by

$$[\mathcal{P}_{2K+1}^{l,m}(\Omega_N^{ij})]_{\text{correlated}} = \mathcal{P}_{2K+1}^{l,m}(\Omega_N^{ij}) \eta(r_{ij}). \quad (19)$$

The potential matrix element $V_{KK'}(r)$ in the CPH basis is now given by

$$V_{KK'}(r) = (h_K^{\alpha\beta} h_{K'}^{\alpha\beta})^{-\frac{1}{2}} \int_{-1}^{+1} \left\{ P_K^{\alpha\beta}(z) V \left(r \sqrt{\frac{1+z}{2}} \right) \times P_{K'}^{\alpha\beta}(z) \eta \left(r \sqrt{\frac{1+z}{2}} \right) W_l(z) \right\} dz. \quad (20)$$

Here, $P_K^{\alpha\beta}(z)$ is the Jacobi polynomial, and its norm and weight function are $h_K^{\alpha\beta}$ and $W_l(z)$, respectively [28].

Note that the inclusion of $\eta(r_{ij})$ makes the CPH basis nonorthogonal. One may surely use the standard procedure for handling the nonorthogonal basis. However, in the present calculation we have checked that $\eta(r_{ij})$ differs from a constant value only in a very narrow interval near the origin, in the BEC length scale a_{ho} (which is much larger than the interatomic interaction length scale). As a result, the overlap matrix becomes a constant matrix for relevant values of r (which is $\sim \sqrt{3N} a_{ho}$). The effect of the constant matrix is taken by a suitable choice of the asymptotic constant C [29].

III. RESULT

A. Choice of two-body potential and calculation of many-body effective potential

As mentioned in the last section, the interatomic potential has been chosen as the van der Waals potential with a hard core of radius r_c , viz., $V(r_{ij}) = \infty$ for $r_{ij} \leq r_c$ and $= -\frac{C_6}{r_{ij}^6}$ for $r_{ij} > r_c$. C_6 is known for a specific atom and in the limit of $C_6 \rightarrow 0$, the potential becomes a hard sphere and the cutoff radius exactly coincides with the s -wave scattering length a_s . By utilizing the Feshbach resonance, one can effectively tune the scattering length a_s . In our choice of two-body potential

we tune r_c to reproduce the experimental scattering length. As we decrease r_c , a_s decreases and at a particular critical value of r_c it passes through an infinite discontinuity, going from $-\infty$ to ∞ [21]. For our present calculation, we choose Rb atoms with $C_6 = 6.4898 \times 10^{-4}$ o.u. [26]. With this $V(r_{ij})$ we solve the zero-energy two-body Schrödinger equation and tune r_c to obtain the a_s correctly. We choose r_c such that it corresponds to the zero node in the zero-energy two-body wave function for $a_s < 0$ and one node for $a_s > 0$ [21,26]. With this set of parameters, we solve the coupled differential equation by hyperspherical adiabatic approximation (HAA) [30]. In HAA, we assume that the hyperradial motion is slow compared to the hyperangular motion and the potential matrix together with the hypercentrifugal repulsion is diagonalized for a fixed value of r . Thus, the effective potential for the hyperradial motion is obtained as a parametric function of r . We choose the lowest eigenpotential $\omega_0(r)$ [the corresponding eigencolumn vector being $\chi_{K0}(r)$] as the effective potential in which the condensate moves collectively. We solve the adiabatically separated hyperradial equation in the extreme adiabatic approximation (EAA)

$$\left[-\frac{\hbar^2}{m} \frac{d^2}{dr^2} + \omega_0(r) - E_R \right] \zeta_0(r) = 0, \quad (21)$$

subject to approximate boundary condition and obtain the hyperradial wave function $\zeta_0(r)$. For our numerical calculation, we fix $l = 0$ and truncate the CPH basis to a maximum value $K = K_{\max}$ requiring proper convergence. Finally, the many-body condensate wave function Ψ can be constructed in terms of $\zeta_0(r)$ and $\chi_{K0}(r)$.

The accuracy of HAA has been tested against exact results for various nuclear and atomic systems. Since exact HHE calculations are possible only for the three-body systems, the tests were done for trinuclei, two-electron atoms, and exotic three-body Coulombic systems. The accuracy was found to be better than 1% even for the infinite-range Coulomb potential [31]. In our calculation, the van der Waals potential has shorter range and hence HAA is expected to be better [30]. Moreover, the confining harmonic potential is smooth and for this potential alone, the hyperradial equation is completely decoupled. Since the trapping potential has a dominant effect, this also improves the accuracy of HAA for application to BEC. For BEC with $N \leq 20$, for which exact DMC results were available, the CPHEM together with HAA were found to be very close to the exact DMC calculations [20]. Moreover, results of our previous BEC calculations using HAA for quite large N agree well with earlier calculations and experiments [14–21,27,29,32,33]. Thus, we can safely use HAA in our calculation and this reduces the numerical complications to a great extent. In addition, the HAA produces an effective hyperradial potential, in which the collective motion takes place.

For the attractive condensate, the many-body effective potential strongly differs from the effective mean-field potential. In GP, the choice of a contact δ interaction in the two-body potential gives rise to the pathological singularity in the effective potential [19,21]. Thus, the study of post-collapse scenario of the attractive condensate is beyond the scope of the GP theory. Whereas the presence of a short-range hard

core in the van der Waals interaction does not only remove the singularity, it gives the realistic scenario and can describe the formation of atomic cluster after the collapse.

B. Information entropy of one-body density

For repulsive BEC, we consider ^{87}Rb atoms in the external spherical harmonic trap of trap frequency 77.87 Hz. The cutoff radius r_c in the van der Waals potential is adjusted to get the scattering length $a_s = 0.00433$ o.u. = $100 a_0$ (a_0 is the Bohr radius) which corresponds to the JILA experiment [7]. For attractive BEC, our choice is ^{85}Rb atoms in the JILA trap with $a_s = -1.832 \times 10^{-4}$ o.u. From the condensate wave function Ψ , we calculate the one-body density $R_1(\vec{r}_k)$ [33] as

$$R_1(\vec{r}_k) = \int_{\tau'} |\Psi|^2 d\tau'. \quad (22)$$

The one-body density basically measures the probability density of finding a particle at a distance \vec{r}_k from the center of mass of the condensate. The integral over the hypervolume τ' excludes the variable \vec{r}_k and $d\tau'$ is given by

$$d\tau' = r'^{3N-4} \cos^2 \phi \sin^{3N-7} \phi dr' d\phi d\omega_{ij} d\Omega_{N-2}, \quad (23)$$

where r' is obtained from $r^2 = r'^2 + 2r_k^2$. After a lengthy but straightforward calculation, we arrive at a close form given by

$$\begin{aligned} R_1(\vec{r}_k) = & \sqrt{2} \int_0^\infty \int_{-1}^1 2^\alpha \left[\frac{1}{\pi^{3/2}} \frac{\Gamma[(D-3)/2]}{\Gamma[(D-6)/2]} \right] [\zeta_0(r')]^2 \\ & \times \sum_{KK'} \chi_{K0}(r') \chi_{K'0}(r') (f_{K1} f_{K'1})^{-1} (h_K^{\alpha\beta} h_{K'}^{\alpha\beta})^{-1/2} \\ & \times P_K^{\alpha\beta}(z) P_{K'}^{\alpha\beta}(z) r'^{D-4} \sqrt{\frac{1+z}{2}} \left(\sqrt{\frac{1-z}{2}} \right)^{D-8} \\ & \times \left(\sqrt{r'^2 + 2r_k^2} \right)^{-(D-1)} dr' dz, \end{aligned} \quad (24)$$

where $D = 3N - 3$ and $h_k^{\alpha,\beta}$ is the norm of the Jacobi polynomial. The integral is computed by numerical computation using a 32-bit Gaussian quadrature. $R_1(\vec{r}_k)$ basically contains all the information of the one-body density correlation. In Fig. 1(a), we plot the one-body density distribution as a function of \vec{r}_k (in o.u.) for several numbers of bosons $N = 50, 500, \text{ and } 5000$. For small-particle number, the density is sharper and with increase in particle number the density distribution gradually pushed out as the effective repulsion increases. Next, taking the Fourier transformation of $R_1(\vec{r}_k)$, we obtain the one-body momentum distribution $\Phi_1(\vec{p}_k)$ and plot in Fig. 1(b) for the same set of particle numbers as in Fig. 1(a). We see the expected reciprocal behavior between the position and momentum space wave function is accordance with the Heisenberg's uncertainty principle. For very small N (~ 100), as the net effective repulsion is small, the condensate wave function is close to Gaussian in both the spaces. However, with increase in N , when the condensate wave function in the coordinate space spreads out due to increase in effective interaction Na_s , the corresponding momentum space wave function squeezes accordingly. Next, to compare our many-body results with the mean field we numerically solve the GP

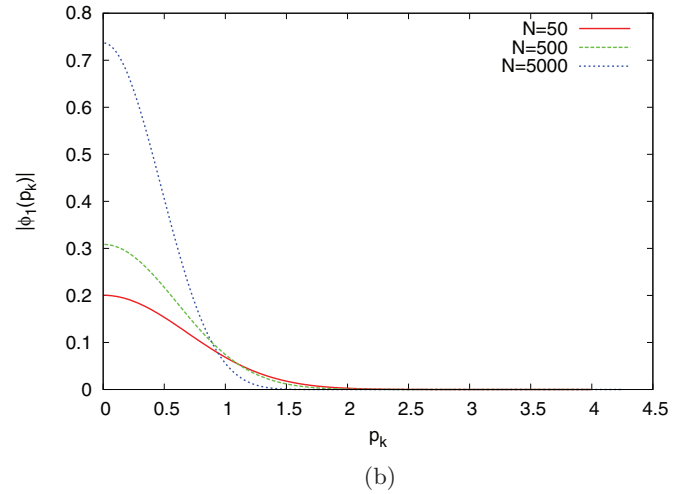
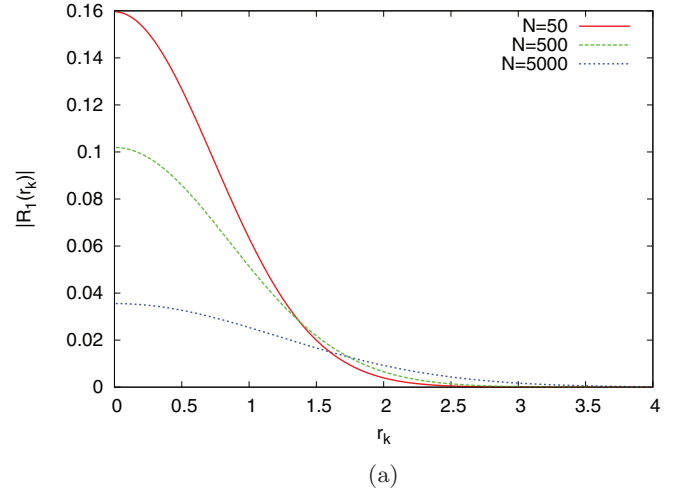


FIG. 1. (Color online) Plot of one-body density as a function of r_k (in o.u.) and the corresponding one-body momentum distribution as a function of p_k (in o.u.) for different N .

equation of the form

$$\left[-\frac{\hbar^2}{2m} \nabla^2 + \frac{1}{2} m \omega^2 r^2 + g |\psi(\vec{r})|^2 \right] \psi(\vec{r}) = \mu \psi(\vec{r}) \quad (25)$$

for the same set of particles as chosen in the many-body calculation. Here, $g = \frac{4\pi\hbar^2 a_s N}{m}$ is the mean-field interaction, m being the mass of the particle. The corresponding one-body density both in the coordinate and momentum spaces are presented in Figs. 2(a) and 2(b), respectively. The expected reciprocal behavior is also seen.

Next, we calculate the Shannon information entropy in the coordinate space using Eq. (1) and the same in momentum space using Eq. (2). In Table I, we present the values of S_r and S_p and the total entropy $S = S_r + S_p$ versus the number of particle N for the ^{87}Rb condensate. For comparison, we also calculate the same for the mean-field and present in Table I.

For small N , the net effective interaction Na_s is very small compared to the trap energy ($\sim \hbar\omega$) and the total entropy is very close to the lower bound of the EUR. However, with increase in particle number N , S smoothly increases. With increase in net repulsive interaction Na_s , the coordinate space

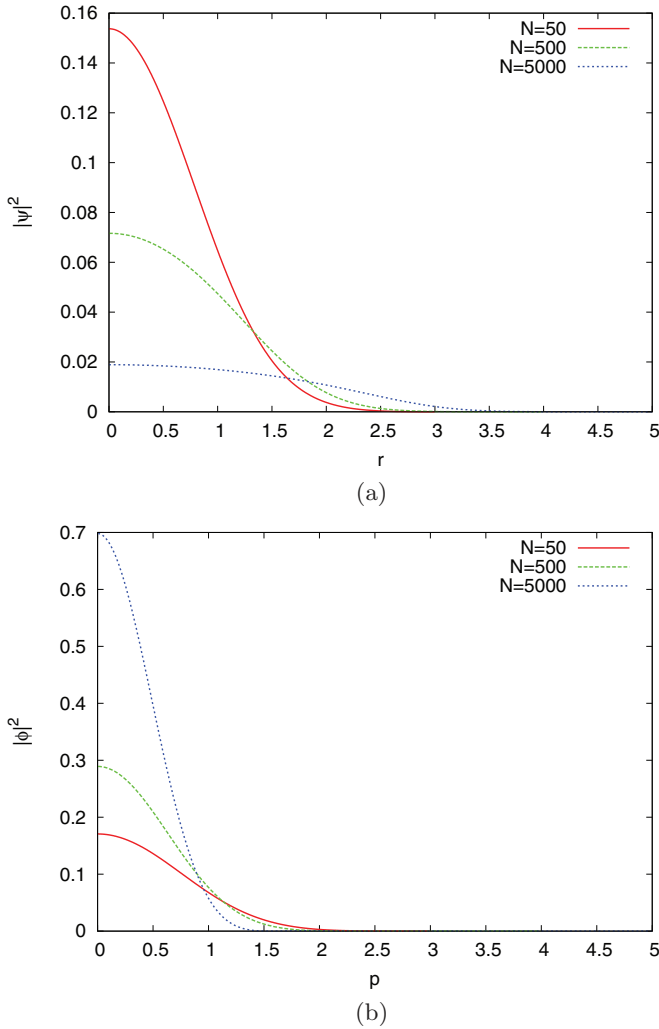


FIG. 2. (Color online) Plot of condensate density $|\psi|^2$ as a function of r (in o.u.) [panel (a)] and the corresponding momentum distributions $|\phi|^2$ as a function of p (in o.u.) [panel (b)] obtained from mean-field GP equation for different N .

wave function delocalizes, consequently, the position space entropy S_r gradually increases. It signifies that the associated uncertainty in the coordinate space increases. The corresponding momentum space wave function is localized, and the associated entropy S_p gradually decreases with increase in $N a_s$. It indicates that the associated uncertainty in momentum

TABLE I. One-body entropy in coordinate space S_r , in momentum space S_p , and total one-body entropy S for some typical N for repulsive BEC. All entropy values are given in o.u.

N	GP theory			CPHEM		
	S_r	S_p	S	S_r	S_p	S
100	3.369	3.087	6.456	3.431	3.004	6.4343
500	3.834	2.630	6.465	3.782	2.653	6.435
1000	4.102	2.398	6.494	4.049	2.389	6.437
3000	4.601	1.968	6.569	4.544	1.921	6.465
5000	4.858	1.750	6.601	4.804	1.674	6.478
7000	5.032	1.620	6.627	4.987	1.495	6.483

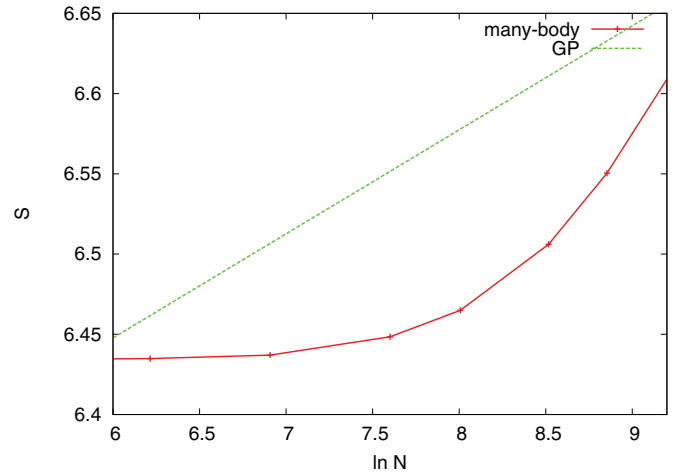


FIG. 3. (Color online) Plot of the one-body entropy S (in o.u.) as a function of $\ln N$. The many-body result is plotted as the red smooth curve and the green dashed curve corresponds to the mean-field GP result.

space decreases. Although we observe the same trend both in the many-body and mean-field results, however, quantitative disagreement occurs. Next, to address the universal relation for Shannon information entropy, we plot it as a function of $\ln N$ in Fig. 3 where our CPHEM result is presented as the red smooth curve and the green dashed curve corresponds to the mean-field GP result. It has been proposed in an earlier calculation [11] that for a system of fermions, the universal relation is maintained and has the form

$$S = a + b \ln N. \quad (26)$$

In the mean-field results (green dashed curve in Fig. 3), we can get back the straight line in the plot of S versus $\ln N$ and the calculated values of $a = 6.059$ and $b = 0.065$. In the many-body calculation, we fail to retrieve the linear relation [Eq. (26)] for the entire particle range. However, in the large-particle limit we observe the straight increase in the total entropy as a function of $\ln N$. It shows that in the small- and finite-particle limits, the many-body calculation exhibits finite-size effect, whereas in the large-particle limit the mean-field results are close to the many-body results for repulsive condensates, as expected.

As pointed out earlier, for repulsive bosons, there is no upper limit of the number of atoms in the trap and the condensate is always stable for any number of atoms. However, in the case of an attractive BEC, the condensate tends to increase its density in the center of the trap in order to lower its interaction energy with increase in the atom number. This tendency is balanced by the zero-point kinetic energy which can stabilize the system. However, for large number of bosons, the central density becomes too high and the kinetic energy can not balance it anymore. The condensate thus collapses beyond a critical number N_{cr} and the corresponding stability factor is defined as $k_{cr} = \frac{N_{cr} |a_s|}{a_{ho}}$. In Fig. 4, we plot S_r and S_p as a function of $N a_s$, where the scattering length a_s is gradually tuned from large repulsive (when the condensate is absolutely stable) to attractive (when the condensate is metastable for smaller $N |a_s|$) and finally collapses at the

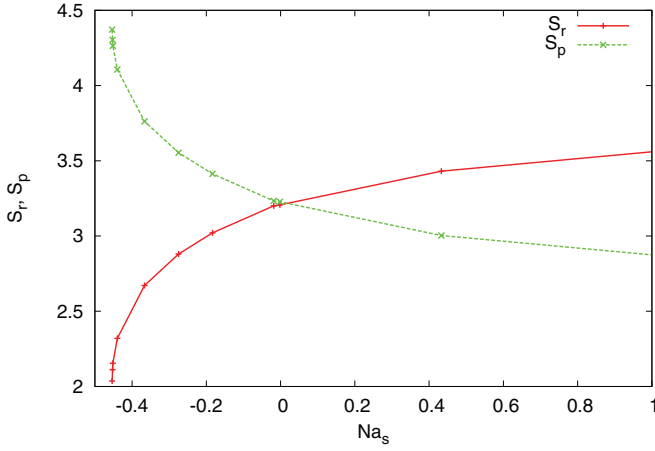


FIG. 4. (Color online) Plot of the one-body entropy in position space S_r (in o.u.) and in momentum space S_p (in o.u.) against effective interaction Na_s in o.u.

criticality). The inverse behavior between the position and momentum space entropies is the consequence of the EUR. At $Na_s = 0$, we reach the noninteracting limit when the system behaves as an ideal Bose gas (IBG). For IBG in a harmonic trap, both the position and momentum space wave functions become perfectly Gaussian. Hence, the Shannon information entropy in position space S_r and that in momentum space S_p become equal to each other and the minimum uncertainty limit is obtained. We have checked the numerical values of S_r and S_p . They are $S_r = S_p = 3.217$; the total entropy $S = 6.434$, which is the lower bound of EUR. However, for attractive BEC, a_s is negative and the condensate is metastable as described earlier. For our present calculation, we keep $a_s = -1.832 \times 10^{-4}$ o.u. which is chosen from the controlled collapse experiment [8,9] and go on increasing N to make more and more attractive condensate. Thus, the condensate density in the coordinate space contracts near the center of the trap, whereas the corresponding momentum space wave function spreads out as expected. It signifies that the associated uncertainty in position space decreases and that in momentum space increases. Thus, with increase in N , S_r starts to fall and S_p starts to increase. At the critical point, the metastable region is no longer able to bound the condensate due to very strong attractive interaction energy. Hence, the condensate wave function in coordinate space squeezes to a δ function and the corresponding momentum space wave function is completely delocalized. This is reflected in a very sharp fall in S_r and very steep increase in S_p (Fig. 4). Thus, at the point of collapse, S_r and S_p diverge in opposite directions. This point of divergence is used to calculate the stability factor which we found to be $k_{cr}^{\text{many-body}} = 0.457$ and is in very close agreement with the experimental value of $k_{cr}^{\text{expt}} = 0.459 \pm 0.012 \pm 0.054$ [8]. In the mean-field GP, the equation stability factor is determined in the following way. When $N < N_{cr}$, the condensate is metastable and the energy functional has a local minimum [25]. When N increases, the depth of local minimum decreases and exactly at $N = N_{cr}$, the minimum vanishes and the GP equation has no solution. The calculated stability factor is $k_{cr}^{\text{GP}} = 0.575$. Thus, our present many-body calculation not only calculates the stability factor

accurately, but also manifests the collapse of the attractive BEC as the simultaneous divergence in S_r and S_p .

C. Information entropy of the two-body density

The two-body Shannon information entropies in position and momentum spaces are defined as [34]

$$S_r = - \int R_2(r_{ij}) \ln R_2(r_{ij}) dr_{ij} \quad (27)$$

and

$$S_p = - \int \Phi_2(p_{ij}) \ln \Phi_2(p_{ij}) dp_{ij}, \quad (28)$$

where $R_2(r_{ij})$ is the two-body density distribution in the coordinate space and the corresponding pair density in momentum space $\Phi_2(p_{ij})$ is obtained by taking Fourier transformation of $R_2(r_{ij})$. The pair-distribution function determines the probability of finding the (ij) th pair at a relative separation r_{ij} in the coordinate space and likewise for the momentum space also. We calculate it as follows:

$$R_2(r_{ij}) = \int_{\tau''} |\Psi|^2 d\tau'', \quad (29)$$

where Ψ is the many-body condensate wave function. As before, τ'' excludes integration over r_{ij} . After a lengthy calculation, we obtain the closed analytic form of $R_2(r_{ij})$ [33] as

$$\begin{aligned} R_2(r_{ij}) = & \sqrt{2} \int_{-1}^1 \left(\frac{1-z}{2} \right)^\alpha \left[\zeta_0 \left(r_{ij} \sqrt{\frac{2}{1+z}} \right) \right]^2 \\ & \times \sum_{KK'} \left(\frac{h_K^{\alpha\beta}}{2^\alpha} \right)^{-1/2} \left(\frac{h_{K'}^{\alpha\beta}}{2^\alpha} \right)^{-1/2} (f_{Kl} f_{K'l})^{-1} \\ & \times \chi_{K0}(r) \chi_{K'0}(r) P_K^{\alpha\beta}(z) P_{K'}^{\alpha\beta}(z) dz. \end{aligned} \quad (30)$$

Taking Fourier transformation of $R_2(r_{ij})$ we get $\Phi_2(p_{ij})$, which gives the pair density in momentum space. Now, utilizing these in Eqs. (27) and (28) we calculate S_r and S_p for various particle number keeping a_s fixed at 0.00433 o.u. for repulsive BEC and at -1.832×10^{-4} o.u. for attractive BEC. We again observe the reciprocal behavior in S_r and S_p . S_r gradually increases with an increase in Na_s and the corresponding S_p gradually decreases. We again observe the diverging behavior in both S_r and S_p near the point of critical instability (Fig. 5). Now, it would be interesting to compare the two-body information entropies with those of one body. We observe overall similar behavior between the one- and two-body quantities, however, quantitative disagreement persists. In Fig. 4, we see that the rate of increase in S_r is not completely balanced by the decrease in S_p , which makes an overall slow increase in the total entropy S . However, in Fig. 5 we observe that although S_r steeply increases with Na_s as in one-body, still the rate of decrease of S_p is very slow. The interatomic interaction with a short-range hard-core repulsion and long-range attractive tail plays an important role here. Especially for the attractive condensate, when the atoms try to form clusters, the strong short-range repulsion comes into play.

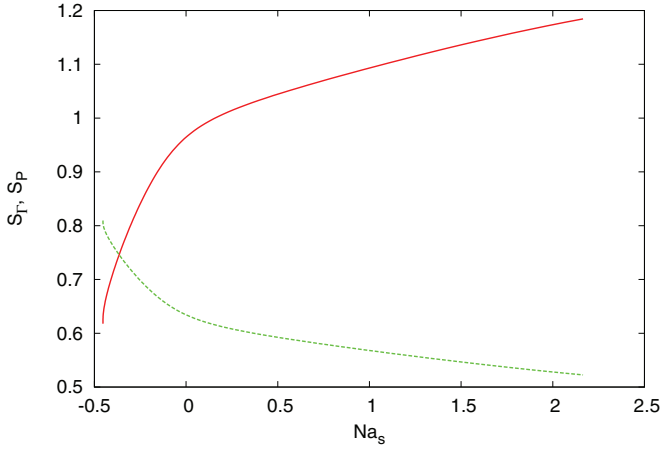


FIG. 5. (Color online) Plot of pair entropy in position space S_r (in o.u.) (red smooth curve) and in momentum space S_p (in o.u.) (green dashed curve) against the effective interaction Na_s (in o.u.).

D. Correlation in dilute BEC

As pointed out earlier for attractive BEC, both the interatomic correlation and realistic interatomic interaction play important roles. Due to the attractive interaction, even in the weakly interacting gas, the effect of correlation becomes important and we expect to get new physics in the study of correlation properties. The mean-field Gross-Pitaevskii (GP) equation with a contact δ interaction is adequate for the description of weakly interacting repulsive Bose gas. However, our correlated basis function is more rigorous and will provide a realistic picture for the study of correlation properties, especially in attractive condensates. To characterize the effect of correlations, in Fig. 6 we plot the pair-distribution function $R_2(r_{ij})$ for the attractive interaction with various particle number. Pair correlation vanishes as $r_{ij} \rightarrow 0$, when the atoms try to form cluster due to strong interatomic correlation, but the strong short-range repulsion tries to separate them. This realistic picture is observed due to the use of realistic interatomic interaction. Again, due to the presence of an external trapping potential, $R_2(r_{ij})$ does not extend beyond the size of the

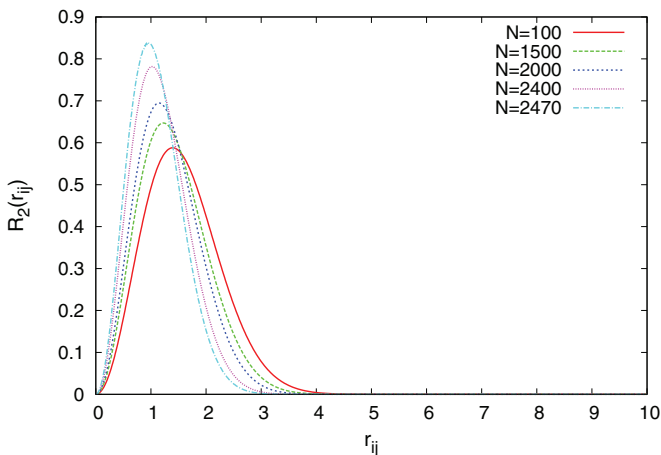


FIG. 6. (Color online) Plot of the pair-distribution functions $R_2(r_{ij})$ as a function of r_{ij} (in o.u.) for different N for attractive BEC.

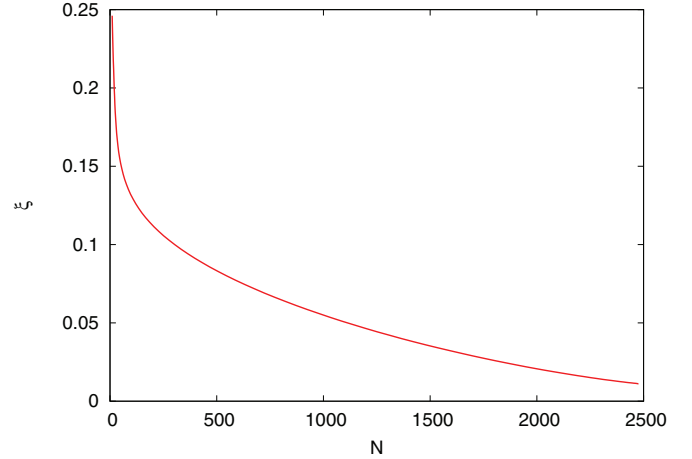


FIG. 7. (Color online) Plot of healing length ξ (in o.u.) with N for attractive BEC.

condensate. Thus, $R_2(r_{ij})$ is peaked at some intermediate value of r_{ij} . Thus, our results are different from the earlier findings of the Lieb-Linger (LL) model which treats one-dimensional *uniform Bose gas*, and particles interact via a δ -function repulsive potential [35,36]. For weak interactions (when the number of particles is much less than the critical number), the correlation length is large, which indicates weak correlation. However, for particle numbers close to the critical point, the condensate becomes strongly correlated, pair-correlation length sharply decreases, and the correlation function becomes sharply localized. It leads to the possibility of formation of atomic clusters due to large two-body correlations. Next, we calculate the healing length ξ , which is considered as the most relevant quantity to quantify the correlation of such highly correlated BEC near the critical point of collapse. It basically measures the minimum distance over which the order parameter can heal [25,26]. We calculate ξ by balancing the quantum pressure and the interaction energy of the condensate and plot it in Fig. 7. ξ steeply decreases with N when the number of atoms is very close to the critical number.

Next, we calculate another useful quantity: the correlation length L . We define L as the half-width of correlation function and plot it in Fig. 8. The smooth decrease in L with the particle number N again confirms the presence of stronger correlations with increase of N in the attractive BEC.

As the attractive condensate becomes highly correlated near the critical point, it is relevant to study its stability by calculating the decay rates due to two- and three-body collisions. The loss rate due to two-body dipolar collisions and three-body recombinations is given by

$$\Gamma = \Gamma_{\text{two}} + \Gamma_{\text{three}} = K_2 \int d\tau |\psi|^4 + K_3 \int d\tau |\psi|^6, \quad (31)$$

where K_2 is the two-body dipolar loss rate coefficient and has the value $(1.87 \pm 0.95 \pm 0.19) \times 10^{-14} \text{ cm}^3/\text{s}$. The three-body recombination loss rate coefficient $K_3 = (4.24_{-0.29}^{+0.70} \pm 0.85) \times 10^{-24} \text{ cm}^6/\text{s}$ [37]. ψ is the condensate wave function in coordinate space and can be calculated as described in Sec. III B. As for an attractive condensate, there is a rapid increase in condensate density with increase in number of atoms, and we may expect a large loss rate near the critical

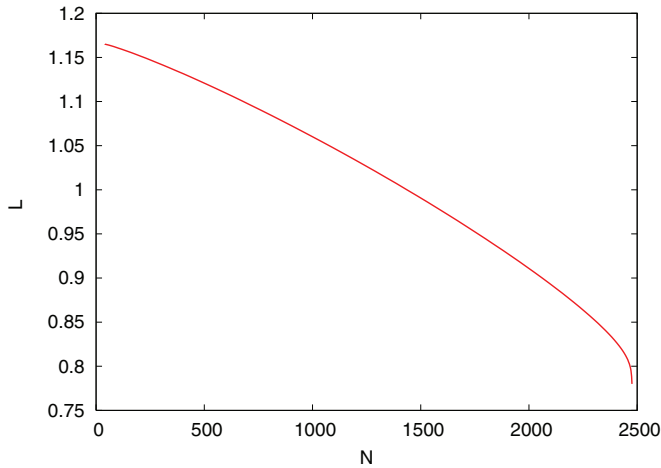


FIG. 8. (Color online) Plot of correlation length L (in o.u.) with N for attractive BEC.

point. It is also important to observe the separate contributions coming from the two-body dipolar loss rate and three-body recombination. In Fig. 9, we plot the two-body dipolar loss rate Γ_{two} and the loss rate due to three-body recombination Γ_{three} . For small particle numbers, as the condensate density is not too high, the three-body loss rate is almost negligible compared to the two-body loss rate. On the other hand, near the critical point when the condensate is highly correlated, we observe a steep increase in the two-body loss rate. The contribution coming from the three-body recombination is still insignificant compared to the sharp change in the dipolar loss rate. Thus, the total loss rate of the attractive condensate is dominated by the two-body loss rate only. This indicates that for the present choices of scattering length of the controlled collapse experiment [8,9], the condensate is sufficiently dilute. Figure 9 also justifies and establishes that in the sufficiently dilute limit, the condensate is affected only by two-body correlations. This also justifies *a posteriori* our use of the two-body correlated basis function (CPH). However, near the Feshbach resonance, where the condensate is strongly correlated the higher-body correlations may significantly contribute and that would be the

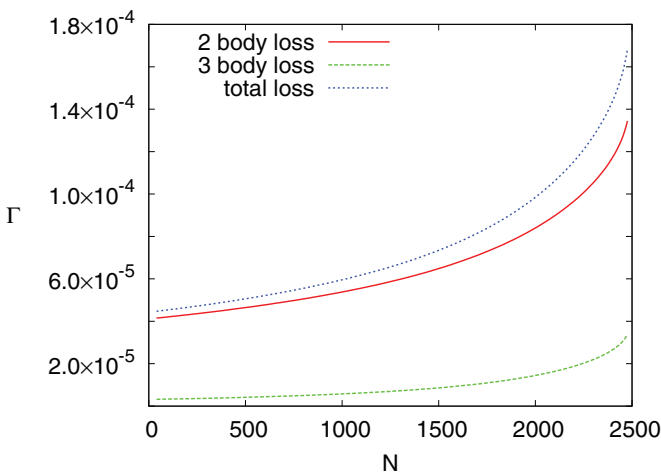


FIG. 9. (Color online) Plot of the loss rate Γ (in atoms/s) due to two- and three-body collisions for various N for attractive BEC.

issue of future research. This is quite obvious from our present study that the effect of three-body recombination is more insignificant for repulsive BEC in the dilute condition. In the repulsive condensate, as the atoms repel each other, the central density is lower and it is less correlated than the attractive condensate. The rate coefficient K_3 is significantly smaller for repulsive condensate. While for the ^{85}Rb condensate (attractive) K_3 is of the order of 10^{-24} cm^6/s , it is of the order of 10^{-30} cm^6/s for the ^{87}Rb condensate (repulsive). This clearly shows the unimportance of the three-body recombination in the context of repulsive BEC.

IV. CONCLUSION

We have reported the results of our numerical calculation on the Shannon information entropy of trapped interacting bosons and study their several characteristic features. We employ two-body correlated basis function and realistic van der Waals interaction. This is the first such rigorous calculation where we observe the interplay between the position and momentum space information entropies. Due to the presence of an external trap, the system is inhomogeneous and gives some additional features. We also numerically establish the lower bound of BBM inequality which is believed to be a stronger version of the Heisenberg uncertainty principle. The observation of curvature in the total entropy S also differs from the earlier mean-field results. Our many-body results show that the finite-size effect is prominent for small and finite numbers of atoms. We also calculate the point of critical instability of attractive BEC. When the number of atoms in the trap is very close to the critical number, the condensate becomes highly correlated and the mean-field GP equation is not enough to describe such a correlated system. Our calculated stability factor is in very close agreement with the experimental results. We observe the point of instability as the point where the information entropies in the conjugate spaces diverge simultaneously. Thus, in our present calculation we not only calculate the instability accurately but at the same time we establish the point in a stronger way providing more information of the BEC as a single quantum entity. We also calculate the two-body Shannon information entropies corresponding to the two-body densities in position and momentum spaces and discuss their similarity and differences with the one-body quantities. Next, we especially discuss the correlation in dilute BEC by introducing several correlation measures such as healing length ξ and correlation length L . We also calculate the two- and three-body loss rate for the attractive condensate. A very sharp increase in the decay rates signifies that near the point of criticality the condensate becomes strongly correlated and there will be a possibility of formation of atomic cluster. All these observations signify quantitatively the presence of interatomic correlations, even away from the critical point in an attractive BEC, which is beyond the scope of studies of mean-field theory.

ACKNOWLEDGMENTS

This work has been supported by Department of Atomic Energy (DAE, India). S.K.H. acknowledges a senior research fellowship from the Council of Scientific and Industrial Research (CSIR), India.

- [1] M. Ohya and P. Petz, *Quantum Entropy and Its Use* (Springer, Berlin, 1993).
- [2] S. E. Massen and C. P. Panos, *Phys. Lett. A* **246**, 530 (1998).
- [3] S. E. Massen and C. P. Panos, *Phys. Lett. A* **280**, 65 (2001).
- [4] C. P. Panos, S. E. Massen, and C. G. Koutroulos, *Phys. Rev. C* **63**, 064307 (2001).
- [5] C. P. Panos, *Phys. Lett. A* **289**, 287 (2001).
- [6] Ch. C. Moustakidis, S. E. Massen, C. P. Panos, M. E. Grypeos, and A. N. Antonov, *Phys. Rev. C* **64**, 014314 (2001).
- [7] M. H. Anderson, J. R. Ensher, M. R. Matthews, C. E. Wieman, and E. A. Cornell, *Science* **269**, 198 (1995).
- [8] J. L. Roberts, N. R. Claussen, S. L. Cornish, E. A. Donley, E. A. Cornell, and C. E. Wieman, *Phys. Rev. Lett.* **86**, 4211 (2001); J. L. Roberts, N. R. Claussen, J. P. Burke, C. H. Greene, E. A. Cornell, and C. E. Wieman, *ibid.* **81**, 5109 (1998).
- [9] S. L. Cornish, N. R. Claussen, J. L. Roberts, E. A. Cornell, and C. E. Wieman, *Phys. Rev. Lett.* **85**, 1795 (2000).
- [10] I. Bialynicki-Birula and J. Mycielski, *Commun. Math. Phys.* **44**, 129 (1975).
- [11] S. E. Massen, Ch. C. Moustakidis, and C. P. Panos, *Phys. Lett. A* **299**, 131 (2002).
- [12] S. Geltman, *Chem. Phys. Lett.* **418**, 163 (2006); *Phys. Lett. A* **356**, 431 (2006); *Mol. Phys.* **106**, 1369 (2008).
- [13] I. Khan and B. Gao, *Phys. Rev. A* **73**, 063619 (2006); B. Gao, *J. Phys. B: At., Mol. Opt. Phys.* **37**, L227 (2004).
- [14] S. K. Haldar, B. Chakrabarti, and T. K. Das, *Phys. Rev. A* **82**, 043616 (2010).
- [15] B. Chakrabarti, T. K. Das, and P. K. Debnath, *Phys. Rev. A* **79**, 053629 (2009).
- [16] P. K. Debnath and B. Chakrabarti, *Phys. Rev. A* **82**, 043614 (2010).
- [17] A. Biswas, B. Chakrabarti, T. K. Das, and L. Salasnich, *Phys. Rev. A* **84**, 043631 (2011).
- [18] A. Biswas, T. K. Das, L. Salasnich, and B. Chakrabarti, *Phys. Rev. A* **82**, 043607 (2010).
- [19] T. K. Das and B. Chakrabarti, *Phys. Rev. A* **70**, 063601 (2004).
- [20] T. K. Das, S. Canuto, A. Kundu, and B. Chakrabarti, *Phys. Rev. A* **75**, 042705 (2007).
- [21] T. K. Das, A. Kundu, S. Canuto, and B. Chakrabarti, *Phys. Lett. A* **373**, 258 (2009).
- [22] M. Fabre de la Ripelle, *Ann. Phys. (NY)* **147**, 281 (1983).
- [23] J. L. Ballot and M. Fabre de la Ripelle, *Ann. Phys. (NY)* **127**, 62 (1980).
- [24] M. Fabre de la Ripelle, *Few-Body Syst.* **1**, 181 (1986).
- [25] F. Dalfovo, S. Giorgini, L. Pitaevskii, and S. Stringari, *Rev. Mod. Phys.* **71**, 463 (1999).
- [26] C. J. Pethick and H. Smith, *Bose-Einstein Condensation in Dilute Gases* (Cambridge University Press, Cambridge, England, 2001).
- [27] B. Chakrabarti and T. K. Das, *Phys. Rev. A* **78**, 063608 (2008).
- [28] M. Abramowitz and I. A. Stegun, *Handbook of Mathematical Functions* (National Institute of Standards and Technology, Washington, DC, 1964).
- [29] S. A. Sofianos, T. K. Das, B. Chakrabarti, M. L. Lekala, R. M. Adam, and G. J. Rampho, *Phys. Rev. A* **87**, 013608 (2013).
- [30] T. K. Das, H. T. Coelho, and M. Fabre de la Ripelle, *Phys. Rev. C* **26**, 2281 (1982).
- [31] V. P. Brito, H. T. Coelho, and T. K. Das, *Phys. Rev. A* **40**, 3346 (1989); S. K. Adhikari, V. P. Brito, H. T. Coelho, and T. K. Das, *Nuovo Cimento B* **107**, 77 (1992); T. K. Das, H. T. Coelho, and V. P. Brito, *Phys. Rev. C* **48**, 2201 (1993); R. Chattopadhyay and T. K. Das, *Phys. Rev. A* **56**, 1281 (1997); T. K. Das and B. Chakrabarti, *Phys. Rev. E* **62**, 4347 (2000); *Int. J. Mod. Phys. A* **19**, 4973 (2004).
- [32] A. Kundu, B. Chakrabarti, T. K. Das, and S. Canuto, *J. Phys. B: At., Mol. Opt. Phys.* **40**, 2225 (2007).
- [33] A. Biswas, B. Chakrabarti, and T. K. Das, *J. Chem. Phys.* **133**, 104502 (2010).
- [34] N. L. Guevara, R. P. Sagar, and R. O. Esquivel, *J. Chem. Phys.* **119**, 7030 (2003).
- [35] E. H. Lieb and W. Liniger, *Phys. Rev.* **130**, 1605 (1963).
- [36] E. H. Lieb, *Phys. Rev.* **130**, 1616 (1963).
- [37] J. L. Roberts, N. R. Claussen, S. L. Cornish, and C. E. Wieman, *Phys. Rev. Lett.* **85**, 728 (2000).